PHYSICAL REVIEW B **87**, 081307(R) (2013)

Raman-scattering measurements and first-principles calculations of strain-induced phonon shifts in monolayer MoS_2

C. Rice, R. J. Young,* R. Zan, and U. Bangert
School of Materials, University of Manchester, Oxford Road, Manchester, M13 9PL, United Kingdom

D. Wolverson
Department of Physics, University of Bath, Claverton Down, Bath, BA2 7AY, United Kingdom

T. Georgiou, R. Jalil, and K. S. Novoselov
School of Physics and Astronomy, University of Manchester, Oxford Road, Manchester, M13 9PL, United Kingdom

(Received 9 November 2012; published 15 February 2013)

The effect of strain on the phonon modes of monolayer and few-layer MoS_2 has been investigated by observing the strain-induced shifts of the Raman-active modes. Uniaxial strain was applied to a sample of thin-layer MoS_2 sandwiched between two layers of optically transparent polymer. The resulting band shifts of the E^1_{2g} ($\sim$385.3 cm^{-1}) and A_{1g} ($\sim$402.4 cm^{-1}) Raman modes were found to be small but observable. First-principles plane-wave calculations based on density functional perturbation theory were used to determine the Grüneisen parameters for the E_{1g}, E^1_{2g}, A_{1g}, and A_{2u} modes and predict the experimentally observed band shifts for the monolayer material. The polymer–MoS_2 interface is found to remain intact through several strain cycles. As an emerging 2D material with potential in future nanoelectronics, these results have important consequences for the incorporation of thin-layer MoS_2 into devices.

DOI: 10.1103/PhysRevB.87.081307 PACS number(s): 78.30.Hv, 62.20.D−, 63.22.−m, 71.15.Mb

Molybdenum disulfide (MoS_2) is a naturally occurring transition-metal dichalcogenide. Its covalently bonded S–Mo–S layers, each of thickness 6.5 Å, experience only a weak inter-layer van der Waals interaction, and can be separated using liquid phase exfoliation,[1] or the Scotch tape technique.[2] As the number of layers of MoS_2 is reduced, the material undergoes a transition from an indirect to a direct band gap semiconductor,[3,4] meaning that monolayer MoS_2 shows a large increase in luminescence quantum efficiency.[5] Monolayer MoS_2 has been shown to have a room-temperature mobility of up to 200 cm^{2}V^{-1}s^{-1}—comparable to that of graphene nanoribbons.[6] Recent work on freely-suspended thin-layer MoS_2 sheets has found that this material has a surprisingly high Young's modulus, $E = 0.33$ TPa,[7] lower than that of graphene with $E = 1.0$ TPa[8] but higher than many other 2D materials such as graphene oxide (0.2 TPa)[9] and hexagonal boron nitride (0.25 TPa).[10] However, unlike graphene, the existence of a band gap in MoS_2, although large at $\sim$1.8 eV for a monolayer,[3] has allowed the fabrication of a monolayer MoS_2 transistor with a room temperature on/off current ratio of 1×10^8.[6] Combining monolayer MoS_2 with graphene in a novel heterostructure[11] has recently been shown to produce a tunneling transistor that retains the high conductivity of graphene, but also has an on/off ratio of 1×10^4.

The presence of strain in low-dimensional materials can have profound effects upon many of the aforementioned properties, and these are important to understand in the context of nanoelectronic devices, and particularly in the search for flexible electronics. Experimental studies on graphene find very large electronic band shifts, and theoretical studies predict the opening of a band gap for large strains[12] and, even, a pseudomagnetic quantum Hall effect for specific strain fields.[13] Here, we report the first study of the effects of uniaxial strain on monolayer MoS_2 and find that the experimentally observed changes are well predicted by first-principles density functional perturbation theory calculations.

Detecting the effects of strain experimentally can be done by observing the phonon modes of the material using Raman spectroscopy, a now well established technique for the study of strain in graphene.[14–16] The Raman spectrum of thin-layer MoS_2 is strongly excitation dependent; resonance excitation ($\sim$1.8–2.0 eV) leads to a rich spectrum of second-order peaks and multiphonon bands[17] due to strong electron-phonon coupling. Away from this resonance, the spectrum becomes simpler; four first-order Raman-active modes can be observed in bulk at approximate frequencies of 32 cm^{-1} (E^2_{2g}), 286 cm^{-1} (E_{1g}, also infrared-active), 383 cm^{-1} (E^1_{2g}), and 408 cm^{-1} (A_{1g}).[18] Figure 1(a) illustrates the atomic displacements giving rise to these modes, along with an infrared active mode with frequency 470 cm^{-1}.

We observe strong Raman signals from the in-plane E^1_{2g} mode, and the out-of-plane A_{1g} mode when exciting with 515 nm excitation, see Fig. 1(b); other modes are not seen here due to difficulty in rejecting Rayleigh scattered laser light (E^2_{2g}), or to selection rules prohibiting their observation in our backscattering experimental arrangement (E_{1g}).[19] As the number of layers of MoS_2 is reduced, the vibrational modes might be expected to soften as the interlayer van der Waals interaction decreases, causing weaker restoring forces in the vibrations. Although this is found to be the case for the A_{1g} mode, surprisingly, an increase in frequency of the E^1_{2g} mode is found, see Fig. 1(b), which is believed to arise from either Coulomb interlayer forces or stacking-induced changes in the intralayer bonding.[20,21] This anomalous behavior is an advantage in identifying the number of layers present in a sample, and in distinguishing from other layer-dependent effects such as sample heating, which softens both modes.

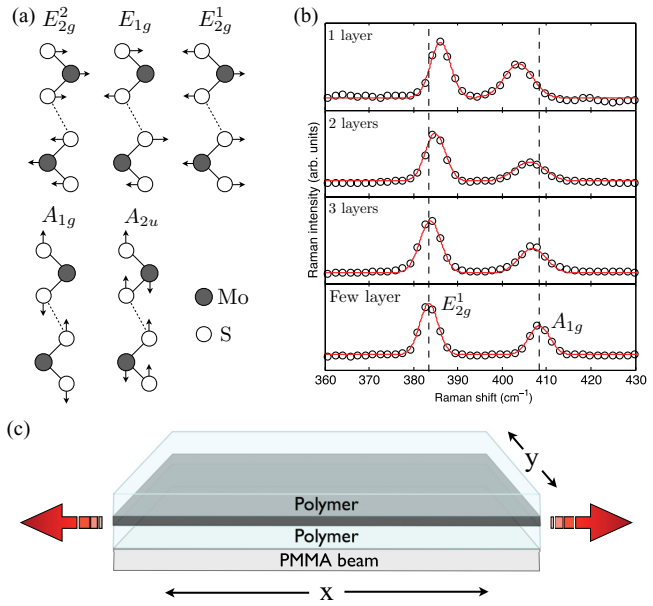

FIG. 1. (Color online) (a) Atomic displacements of the Raman and infrared active modes. (b) Raman spectra of MoS_2, showing the evolution of peak position of the E^1_{2g} and A_{1g} modes for varying layer thicknesses. Open circles show the experimental data, and solid red lines show Gaussian fits indicating inhomogeneous peak broadening, possibly due to small variations in strain. (c) Schematic (not to scale) of the experimental setup, discussed in the text. Red arrows indicate the direction of the applied strain.

MoS_2 specimens were prepared using mechanical cleavage and the microstructures of the cleaved materials were evaluated using a Tecnai F30 transmission electron microscope (TEM) operated at 300 kV. The high-resolution phase contrast TEM image in Fig. 2(a) is of monolayer MoS_2, showing the atomic lattice structure with overlying wormlike contrast arising from the ubiquitous hydrocarbon contamination. The

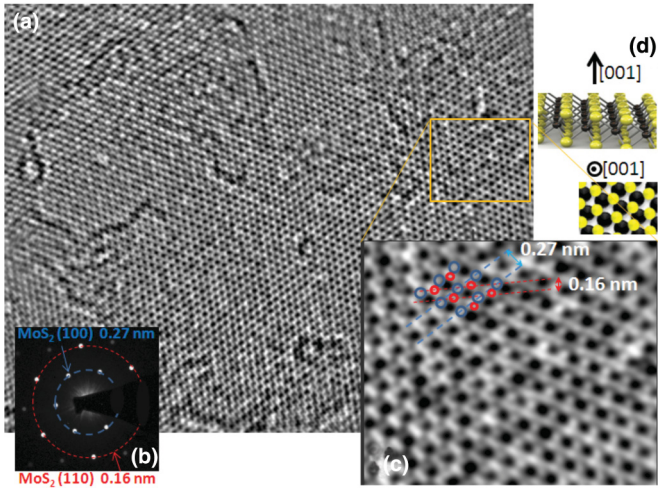

FIG. 2. (Color online) (a) Lattice resolution TEM image of a $\sim 25 \times 20$ nm^2 area of monolayer MoS_2 revealing hydrocarbon contamination as a wormlike background contrast. (b) Electron diffraction pattern of monolayer MoS_2. (c) A magnified area from (a), showing the atom arrangements similar to the [001] view in the model shown in (d).

right-hand inset [see Fig. 2(c)] is an enlarged view of the boxed area; the image has been Fourier filtered in order to remove high-frequency noise. Overlaid in ball-and-stick model fashion is a schematic of a [001] view showing the atomic sublattices represented by different colored circles [also seen in the crystal structure ball-and-stick models in Fig. 2(d)]. The existence of the two sub-lattices and their atomic arrangements becomes quite obvious from the image contrast in the enlarged section [see Fig. 2(c)], even without determining which of the sublattices gives rise to the particular contrast periodicities. It was found that the monolayers were sensitive to the electron beam at this voltage (300 kV) upon prolonged exposure. Because of this, after optimizing the focusing conditions, images were obtained from adjacent regions that had not previously been exposed, and a repeat image was obtained immediately to ensure that no changes had taken place during the exposure. The electron diffraction pattern of monolayer MoS_2 is shown in Fig. 2(b). The black shape is the beam stop. The diffraction pattern consists of two rings, signifying the (100)- and (110)-type lattice plane spacings of the respective 3D crystal structures that exhibited no change in intensity upon tilting. This behavior is characteristic for single-layer flakes of MoS_2, where the $\neq 1$ intensity ratio (in this case ~ 0.87) of neighboring 100-type diffraction spots, has been reported by Brivio *et al.*[22] as being due to symmetry breaking.

In order to study strain effects, the thin layer MoS_2 flakes were deposited onto a PMMA beam spin-coated with SU-8 polymer. The sample was capped on top with a second layer of SU-8 polymer, as shown in Fig. 1(c), and then cured so that the polymer is optically transparent. An area of monolayer MoS_2, ~ 20 μm in length, was identified and measurements taken for three central parts in close proximity. All three monolayer areas studied gave similar results and so the spectra were obtained for one of these areas only. Uniaxial strain was applied to the PMMA beam using a 4-point bending rig. The amount of strain applied was calibrated using a resistance strain gage (gage factor is 2.08) attached using cyanoacrylate adhesive to the sample, and which was positioned as close as possible to the area being studied. Strain was applied in steps of 0.05% up to a maximum of 0.7%. The size of the MoS_2 flakes studied was several orders of magnitude thinner than the thickness of the PMMA beam and so the strain in the middle of the flakes can be assumed to be the same as the strain in the PMMA, given by the strain gage, as has been found for similar experiments upon graphene.[14–16]

Raman spectroscopy was undertaken with an excitation wavelength of 514.5 nm (2.4 eV), using a Renishaw 1000 spectrometer, with 50× microscope objective. The laser power was kept low, <1 mW, to avoid sample damage. For all data shown, the incident light was polarized either parallel or perpendicular to the direction of the applied strain, and the scattered light was left unanalyzed. The data were found to be fully reproducible over several strain cycles up to 0.7% indicating no breakdown or decoupling of the polymer–MoS_2 interface.

Computational studies of the lattice dynamics and elastic properties of MoS_2 have been carried out by several groups, using valence force-field[23] and *ab initio* methods[20,24–27] though, as far as we are aware, there have been no investigations of the strain dependence of the phonon modes. *Ab initio* methods have been very successful at reproducing the measured phonon

dispersion of MoS_2[24] and so we use first-principles plane-wave calculations based on density functional perturbation theory (DFPT)[28] to obtain the frequencies of the phonon modes at the Brillouin zone center as a function of in-plane strain. We use DFPT as implemented in the QUANTUM ESPRESSO package[29] with ultrasoft pseudopotentials.[30,31] The exchange correlation potential was represented in the generalized gradient approximation using a Perdew-Wang functional (GGA-PW91),[32] as in earlier studies.[24,26] Layers in the three-dimensional supercell were spaced by at least 10 Å to ensure there was no interaction between them and so no van der Waals corrections were required. Convergence of the total energy was checked with respect to the kinetic energy cutoff (70 Ry) and Brillouin zone sampling (a $25\times25\times1$ Monkhorst-Pack grid was used).[33] The optimized lattice parameter a was found to be 3.2132 Å, which agrees to better than 2% with the experimental value of 3.16 Å.[34]

Two types of distortion of the planar lattice were applied; a symmetry-preserving isotropic expansion ("hydrostatic") and a shear distortion ("shear"), which preserves area.[35] In both cases, the positions of the Mo atoms were fixed to obtain the required unit cell parameters but the S atoms were allowed to relax in the z (hydrostatic) and x,y,z (shear) directions to minimize the forces on them before calculation of the lattice modes. The maximum strains used were of order 0.5% and so no adjustment to the density of k-point sampling was necessary. As a further test, the in-plane stiffness was calculated from the variation of the total energy as a function of hydrostatic distortion (after relaxation of the S atoms) and was 160 Nm^{-1}, which compares well to other calculated values (e.g., 146 Nm^{-1})[24] and experiment (180 ± 60 Nm^{-1}).[36]

Figure 3 shows the position of the experimentally measured E^1_{2g} and A_{1g} Raman peaks as uniaxial strain is applied, for both a monolayer area and a few-layer flake. The spectra were fitted with Gaussians, as shown in Fig. 1. The resulting peak positions as a function of strain have been fitted linearly, shown by dashed lines in Fig. 3. We observe a very small shift of the A_{1g} mode to lower frequency for both monolayer and few-layer areas at a rate of -0.4 cm^{-1} per % strain. The E^1_{2g} mode, however, shows a considerably larger shift, with the monolayer rate greatest at -2.1 cm^{-1} per % strain, and the few-layer slightly lower at -1.7 cm^{-1} per % strain. The observation of a lower rate for few-layer material compared to monolayer material has also been observed in graphene, where studies on

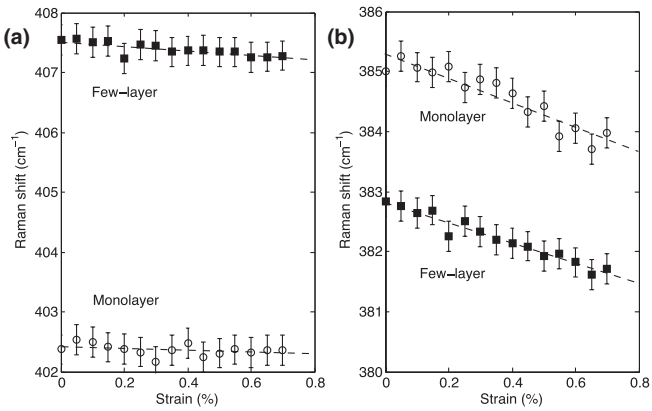

FIG. 3. Position of the (a) A_{1g} and (b) E^1_{2g} Raman peaks from monolayer (open circles) and few-layer (filled squares) MoS_2. Dashed lines are linear fits to the data discussed in the text. Error bars indicate the spectrometer resolution.

capped and uncapped samples of different thicknesses indicate that this is not due to poor adhesion with the substrate, and is instead an inherent property of the few-layer material.[16]

To derive the phonon shift for uniaxial strain we follow the method of Ref. 37 and our results are illustrated in Ref. 38. For the hydrostatic case, modes of symmetry type E (in-plane displacements) and type A (out-of-plane displacements) all shift to lower frequency ω as the lattice expands with a rate which is given by the Grüneisen parameter γ_m for a phonon mode m:

$$\gamma_m = -\frac{1}{\omega_m}\frac{\partial\omega_m}{\partial\epsilon}, \tag{1}$$

where the strain $\epsilon=\epsilon_x+\epsilon_y$.

In the case of a pure shear strain, we expect on symmetry grounds that the modes of type A should be (to a first approximation) unaffected whilst the reduction of the lattice symmetry from D_{3h} will lift the degeneracy of the E modes. For each E mode, two components will appear, which should shift equally up and down in frequency with a rate β_m that is defined as γ_m in Eq. (1) but now with $\epsilon=\epsilon_x-\epsilon_y$. The frequency values ω_m and γ_m, β_m that we find for each mode are given in Table I.

To simulate the experimental results, we derive the phonon shift for modes of E and A symmetry using the fact that

TABLE I. DFPT results compared to experimental data for monolayer MoS_2. Experimental results are those found in this work, except where a reference is given.

	E_{1g}	E^1_{2g}	A_{1g}	A_{2u}
ω (cm^{-1}) (Expt.)	287[a]	385.3	402.4	470.0[b]
ω (cm^{-1}) (DFPT)	278.1	376.18	397.83	460.7
γ (per % strain)	0.54	0.65	0.21	0.53
β (per % strain)	0.24	0.34	−0.01	−0.01
$\Delta\omega/\epsilon$ (cm^{-1} per % strain) (Expt.)	not seen[c]	−2.1	−0.4	not seen[d]
$\Delta\omega/\epsilon$ (cm^{-1} per % strain) (DFPT)	−1.32, −0.64	−2.22, −0.32	−0.55	−1.58

[a]Reference 23.
[b]Reference 18.
[c]Prohibited by selection rules in our geometry, see Ref. 19.
[d]Infrared-active only.

for uniaxial strain $\epsilon_x = \epsilon$ and $\epsilon_y = -\nu\epsilon$, where ν is Poisson's ratio. Since the MoS_2 is coated on both sides by SU-8 polymer, we take the value of $\nu = 0.35$, as appropriate for the polymer, and not MoS_2, and which has been successful in modeling similar graphene samples.[37] In Table I, the experimental results and theoretical predictions are compared. The agreement of the DFPT calculations and experiment is good for the Γ-point phonon frequencies, as found by others.[24,26] The predictions for the rate of change of these modes with strain, -2.22 cm^{-1} per % strain and -0.55 cm^{-1} per % strain for the E^1_{2g} and A_{1g} modes, respectively, are also in good agreement with the corresponding measured values of -2.1 cm^{-1} per % strain and -0.4 cm^{-1} per % strain. We therefore conclude that DFPT methods are well suited to this material and could be used to make further physical predictions.

Experimentally, we have not been able to observe a splitting of the doubly degenerate E^1_{2g} mode, the two components of which are expected to be orthogonally polarized. It is possible that we are limited by the resolution of our system because we do, however, observe a considerable broadening of this mode, shown in Ref. 38, not seen for the A_{1g} mode, which could indicate an unresolved splitting. We also consider the possibility of a nonuniform strain distribution within the illuminated area, which would lead to a larger range of Raman shifts for the E^1_{2g} peak given its larger shift rate. A full spatial mapping of the strain distribution across thin flakes would give an indication of the magnitude of the variations. The apparent narrowing of the A_{1g} mode is yet to be understood, and further experiments are needed to determine any effects of the crystal orientation in reference to the strain and light polarization axes.

In summary, we have observed uniaxial strain-induced phonon shifts in monolayer and few-layer MoS_2 using Raman spectroscopy. Due to the scaling of the Grüneisen parameter with frequency, see Eq. (1), the shifts observed with strain are small compared with those seen for the G and D peaks of graphene and similar materials.[14–16,37] Despite this, we are able to observe changes in the peak positions of both the E^1_{2g} and A_{1g} modes and find that our DFPT calculations predict these shifts well. The polymer–MoS_2 interface is found to remain intact over several strain cycles. As well as quantifying the effects of uniaxial stress on an MoS_2 monolayer, these results have important consequences for the incorporation of this material into future nanoelectronic devices.

CR was supported by the EPSRC through grant number EP/F028431/1. The overall programme of research was supported by the EPSRC and the Royal Society. The computational work was performed on the University of Bath's High Performance Computing Facility.

*Corresponding author: robert.young@manchester.ac.uk

[1] P. Joensen, R. F. Frindt, and S. R. Morrison, Mater. Res. Bull. **21**, 457 (1986).
[2] K. S. Novoselov, D. Jiang, F. Schedin, T. J. Booth, V. V. Khotkevich, S. V. Morozov, and A. K. Geim, Proc. Natl. Acad. Sci. USA **102**, 10451 (2005).
[3] K. F. Mak, C. Lee, J. Hone, J. Shan, and T. F. Heinz, Phys. Rev. Lett. **105**, 136805 (2010).
[4] A. Kuc, N. Zibouche, and T. Heine, Phys. Rev. B **83**, 245213 (2011).
[5] A. Splendiani, L. Sun, Y. Zhang, T. Li, J. Kim, C.-Y. Chim, G. Galli, and F. Wang, Nano Lett. **10**, 1271 (2010).
[6] B. Radisavljevic, A. Radenovic, J. Brivio, V. Giacometti, and A. Kis, Nature Nanotechnology **6**, 147 (2011).
[7] A. Castellanos-Gomez, M. Poot, G. A. Steele, H. S. J. van der Zant, N. Agraït, and G. Rubio-Bollinger, Adv. Mater. **24**, 772 (2012).
[8] C. Lee, X. Wei, J. W. Kysar, and J. Hone, Science **321**, 385 (2008).
[9] C. Gómez-Navarro, M. Burghard, and K. Kern, Nano Lett. **8**, 2045 (2008).
[10] L. Song, L. Ci, H. Lu, P. B. Sorokin, C. Jin, J. Ni, A. G. Kvashnin, D. G. Kvashnin, J. Lou, B. I. Yakobson, and P. M. Ajayan, Nano Lett. **10**, 3209 (2010).
[11] L. Britnell, R. V. Gorbachev, R. Jalil, B. D. Belle, F. Schedin, A. Mishchenko, T. Georgiou, M. I. Katsnelson, L. Eaves, S. V. Morozov, N. M. R. Peres, J. Leist, A. K. Geim, K. S. Novoselov, and L. A. Ponomarenko, Science **335**, 947 (2012).
[12] V. M. Pereira, A. H. Castro Neto, and N. M. R. Peres, Phys. Rev. B **80**, 045401 (2009).
[13] F. Guinea, M. I. Katsnelson, and A. K. Geim, Nat. Phys. **6**, 30 (2009).
[14] L. Gong, I. A. Kinloch, R. J. Young, I. Riaz, R. Jalil, and K. S. Novoselov, Adv. Mater. **22**, 2694 (2010).
[15] R. J. Young, L. Gong, I. Kinloch, I. Riaz, R. Jalil, and K. S. Novoselov, ACS Nano **5**, 3079 (2011).
[16] L. Gong, R. J. Young, I. A. Kinloch, I. Riaz, R. Jalil, and K. S. Novoselov, ACS Nano **6**, 2086 (2012).
[17] A. M. Stacy and D. T. Hodul, J. Phys. Chem. Solids **46**, 405 (1985).
[18] T. Wieting and J. Verble, Phys. Rev. B **3**, 4286 (1971).
[19] J. L. Verble and T. J. Wieting, Phys. Rev. Lett. **25**, 362 (1970).
[20] C. Lee, H. Yan, L. E. Brus, T. F. Heinz, J. Hone, and S. Ryu, ACS Nano **4**, 2695 (2010).
[21] H. Li, Q. Zhang, C. C. R. Yap, B. K. Tay, T. H. T. Edwin, A. Olivier, and D. Baillargeat, Adv. Funct. Mater. **22**, 1385 (2012).
[22] J. Brivio, D. T. L. Alexander, and A. Kis, Nano Lett. **11**, 5148 (2011).
[23] S. J. Sandoval, D. Yang, R. F. Frindt, and J. C. Irwin, Phys. Rev. B **44**, 3955 (1991).
[24] C. Ataca, M. Topsakal, E. Aktürk, and S. Ciraci, J. Phys. Chem. C **115**, 16354 (2011).
[25] A. Molina-Sánchez and L. Wirtz, Phys. Rev. B **84**, 155413 (2011).
[26] Q. Yue, J. Kang, Z. Shao, X. Zhang, S. Chang, G. Wang, S. Qin, and J. Li, Phys. Lett. A **376**, 1166 (2012).
[27] K. Kaasbjerg, K. S. Thygesen, and K. W. Jacobsen, Phys. Rev. B **85**, 115317 (2012).
[28] P. Giannozzi, S. De Gironcoli, P. Pavone, and S. Baroni, Phys. Rev. B **43**, 7231 (1991).
[29] P. Giannozzi, S. Baroni, N. Bonini, M. Calandra, R. Car, C. Cavazzoni, D. Ceresoli, G. L. Chiarotti, M. Cococcioni, I. Dabo, A. Dal Corso, S. de Gironcoli, S. Fabris, G. Fratesi, R. Gebauer, U. Gerstmann, C. Gougoussis, A. Kokalj, M. Lazzeri, L. Martin-Samos, N. Marzari, F. Mauri, R. Mazzarello, S. Paolini, A. Pasquarello, L. Paulatto, C. Sbraccia, S. Scandolo, G. Sclauzero, A. P. Seitsonen, A. Smogunov, P. Umari, and R. M. Wentzcovitch, J. Phys.: Condens. Matter **21**, 395502 (2009).

[30]D. Vanderbilt, Phys. Rev. B **41**, 7892 (1990).

[31]We used Mo.pw91-n-van.UPF and S.pw91-van_ak.UPF from http://www.quantum-espresso.org.

[32]J. P. Perdew, J. A. Chevary, S. H. Vosko, K. A. Jackson, M. R. Pederson, D. J. Singh, and C. Fiolhais, Phys. Rev. B **46**, 6671 (1992).

[33]H. J. Monkhorst and J. D. Pack, Phys. Rev. B **13**, 5188 (1976).

[34]J. A. Wilson and A. D. Yoffe, Adv. Phys. **18**, 193 (1969).

[35]C. Thomsen, S. Reich, and P. Ordejón, Phys. Rev. B **65**, 073403 (2002).

[36]S. Bertolazzi, J. Brivio, and A. Kis, ACS Nano **5**, 9703 (2011).

[37]T. M. G. Mohiuddin, A. Lombardo, R. R. Nair, A. Bonetti, G. Savini, R. Jalil, N. Bonini, D. M. Basko, C. Galiotis, N. Marzari, K. S. Novoselov, A. K. Geim, and A. C. Ferrari, Phys. Rev. B **79**, 205433 (2009).

[38]See Supplemental Material at http://link.aps.org/supplemental/10.1103/PhysRevB.87.081307 for full DFPT results and graphs of the Raman peak widths.